Vol. 08, No. 1 (2026) 417-428, doi: 10.24874/PES08.01A.014

Proceedings on Engineering Sciences

www.pesjournal.net

PARAMETRIC STUDY ON THE INFLUENCE OF TENDON DIAMETER AND SLAB DEPTH ON THE LOAD-BEARING CAPACITY OF PRESTRESSED HOLLOW-CORE SLABS

Mohamed A. El Awady
Abdelrahman Elsaid
Mohamed Abdelhakim Basal[1]

Received 05.12.2025
Revised 15.01.2026
Accepted 10.02.2026

Keywords:

Prestressed concrete, Hollow-core slab, Tendon diameter, Cracking moment, Flexural resistance, Compression depth, Numerical modeling.

A B S T R A C T

This work evaluates how tendon size distribution and member depth affect the flexural performance of prestressed hollow-core slabs, with the total prestressing steel area kept constant. A parametric numerical program was carried out in Concise Beam, considering tendon diameters of 5, 10, 15, and 20 mm and slab depths of 200, 320, and 400 mm, subjected to a single point load at midspan. For each configuration, the cracking moment, ultimate flexural capacity, and the depth of the compression zone were extracted to quantify the effect of changing tendon diameter at equal steel area. To check the numerical predictions, independent calculations were implemented in MATLAB, showing close agreement with the software output. The analyses consistently show that using multiple medium-diameter tendons (10 mm) yields the most favorable response, producing higher cracking and resistance moments and a more effective compression-zone development. In contrast, larger individual strands (15–20 mm) lead to lower flexural efficiency even when the steel area is unchanged, suggesting that concentrating prestress into fewer larger tendons is less advantageous. These results support the use of distributed prestressing layouts in precast hollow-core systems and motivate further research on how tendon spacing and slab width govern the prestress influence region.

1. INTRODUCTION

Prestressed hollow-core slabs are widely used in modern floor systems because they provide an efficient way to achieve long spans with relatively low self-weight. The hollow geometry reduces concrete volume, while prestressing improves tensile capacity and delays cracking. These characteristics make hollow-core units attractive for buildings that require fast construction and repetitive structural layouts.

Although hollow-core slabs share similarities with solid prestressed members, their structural behavior is not identical. The presence of webs and voids influences stiffness distribution, cracking patterns, and internal force transfer. As a result, predictions of flexural and

[1] Corresponding author: Mohamed Abdelhakim Basal
Email: mohamedabdelhikeem@yahoo.com

shear behavior based on models developed for solid sections may not always be directly applicable to hollow-core members, especially when prestressing arrangements or tendon properties are modified.

Long-term effects further complicate the response of prestressed slabs. Prestress losses caused by creep, shrinkage, and steel relaxation change stress levels within the member and can influence deflection and cracking under service loads. These losses also affect the available margin between serviceability and ultimate limit states (He et al., 2024). Therefore, choices related to slab geometry and tendon configuration play an important role in both service performance and structural safety.

In this study, a parametric numerical investigation is conducted to examine the influence of slab depth and tendon diameter on the flexural behavior of prestressed hollow-core slabs while keeping the total prestressing steel area constant. Parameters associated with serviceability and strength, including cracking moment, ultimate bending moment, and compression zone depth, are evaluated. The numerical analyses are performed using independently developed routines implemented in MATLAB (2023). The aim is to provide practical guidance on tendon arrangement that improves structural efficiency without increasing material usage.

2. LITERATURE REVIEW

Several studies have addressed different aspects of the behavior of prestressed hollow-core slabs, reflecting their widespread use and structural importance. Research has shown that their performance is affected by multiple interacting parameters rather than by a single dominant factor.

Prestress loss is one of the most important issues influencing service behavior. Reductions in prestressing force overtime alter stress distributions and increase the likelihood of cracking under working loads. He et al. (2024) reported that prestress losses have a noticeable impact on service stresses and deflections and should be considered carefully when evaluating long-term performance.

Other researchers have examined hollow-core slabs under conditions that deviate from standard design assumptions, such as elevated temperatures or unconventional loading scenarios. These studies indicate that stiffness degradation, cracking development, and failure modes can differ from those predicted by simplified analytical models (McGinnis et al., 2024).

Attention has also been given to the influence of geometric configuration and prestressing characteristics on flexural capacity. Variations in web geometry, void arrangement, and tendon properties have been shown to affect cracking behavior and ultimate resistance. Hasib et al. (2025) demonstrated that changes in prestressing characteristics can lead to noticeable differences in flexural response, even when the total amount of prestressing steel remains similar.

Overall, the existing literature suggests that further parametric studies are needed to isolate the influence of individual design variables on the behavior of prestressed hollow-core slabs. In particular, limited information is available on the effect of tendon diameter when the total prestressing steel area is kept constant across different slab depths. The present study addresses this gap.

3. NUMERICAL MODELLING AND METHODOLOGY

3.1 Overview of the Numerical Program

This study evaluates the influence of tendon diameter on the flexural behaviour of prestressed hollow-core slabs (HCS) while maintaining a constant total prestressing steel area. Four tendon diameters 5, 10, 15, and 20 mm are examined for three slab depths (200, 320, and 400 mm). Numerical analyses are performed using Concise Beam, and independent MATLAB (2023) sectional-analysis routines are used for validation.

All slabs are modelled as composite sections composed of a precast hollow-core unit topped with cast-in-place concrete.

The primary performance indicators evaluated are:
• cracking moment (M_{cr}),
• ultimate resistance moment (M_r), and
• compression-zone depth (c).

3.2 Slab Configurations and Loading Conditions

3.2.1 Slab Depths and Tendon Configurations

Three slab depths representative of common precast production practice were considered in the numerical program, namely 200 mm, 320 mm, and 400 mm. For each slab depth, four tendon diameters (5, 10, 15, and 20 mm) were examined while maintaining a constant total prestressing steel area. This modelling strategy ensures that any observed variation in structural response can be attributed exclusively to the effect of tendon diameter and its resulting distribution within the cross-section, rather than to changes in the total amount of prestressing steel.

Across all configurations, modifying the tendon diameter alters only the number of tendons, their spacing and distribution, and the degree of prestress concentration within the section, without affecting the total prestressing force or steel area. This approach allows the isolated influence of tendon diameter on flexural behaviour to be evaluated in a clear and systematic manner. A summary of the investigated slab configurations and key modelling parameters is provided in Table 1.

As shown in Table 2, the total prestressing steel area was maintained approximately constant for all tendon diameters, with values ranging between 1256 and 1287 mm². The selected tendon diameters include standard commercial strand sizes (e.g., 9.5 mm and 15.2 mm corresponding to nominal 3/8 in and 0.6 in strands); rounded nominal metric equivalents are provided for clarity**.** This small variation reflects commercially available strand sizes and does not affect the comparative nature of the study. By keeping the total steel area constant, the influence of tendon diameter is isolated from the effects of prestressing force magnitude, allowing a direct assessment of how strand number and distribution govern cracking behaviour, flexural resistance, and compression-zone development.

Table 1. Summary of investigated slab configurations.

Parameter	Values
Slab depth (mm)	200, 320, 400
Tendon diameter (mm)	5, 10, 15, 20
Total prestressing steel area	Constant
Loading case	Single mid-span concentrated load
Analysis method	Concise Beam and MATLAB

Table 2. Prestressing tendon configurations adopted in the numerical study.

Tendon diameter (mm)	No. of strands	Area per strand (mm^2)	Total steel area (mm^2)	Steel grade (MPa)	Jacking level (%fpu)	Tendon eccentricity (mm)	Tendon profile
5.0	65	19.6	1274	1700	75%	87	Straight
9.5 mm (nominal 10 mm)	23	55.0	1265	1850	75%	87	Straight
15.2 mm (nominal 15 mm)	9	143.0	1287	1790	75%	87	Straight
20.0	4	314.0	1256	1790	75%	87	Straight

3.2.2 Loading Scenario

To focus the analysis on the critical flexural condition of HCS, a single loading case is adopted: 50 KN concentrated load applied at mid-span (L/2). This scenario represents the standard benchmark for evaluating cracking and flexural resistance and avoids unnecessary duplication of results.

3.3 Material Properties

3.3.1 Concrete Properties

The mechanical properties of the precast and cast-in-place concrete layers are summarized in Table 3 and were directly implemented in Concise Beam, including strength values at transfer, lifting, and service stages. The concrete material properties adopted in the numerical models were selected in accordance with EN 1992-1-1 (Eurocode 2), with elastic modulus and tensile strength values calculated based on the characteristic compressive strength in accordance with Clauses 3.1.2–3.1.4. These properties govern cracking behaviour and nonlinear sectional response.

Table 2. Concrete material properties according to EN 1992-1-1 (Eurocode 2), Section 3.1.

Property	Precast Concrete	Cast-in-Place Concrete
Density	2500 kg/m³	2400 kg/m³
$f'c$	50.0 MPa	30.0 MPa
Flexural tensile strength (fr)	4.24 MPa	3.29 MPa
Elastic modulus (Ec)	34,263 MPa	26,621 MPa
Strength at transfer ($f'c$)	28.0 MPa	–
Ec at transfer	27,608 MPa	–
Strength in lifting	30.0 MPa	–
Ec at lifting	28,302 MPa	–

3.3.2 Precast Concrete Mix and Environmental Conditions

The precast concrete mix design and service-environment parameters adopted in the numerical modelling were selected to be representative of typical precast hollow-core production practice. These parameters were incorporated in the Concise Beam material definitions to account for shrinkage development, curing conditions, and service-stage environmental effects.

The adopted mix included a cement content of 410 kg/m³ with an air content of 5% and a slump of 50 mm. The aggregate system was characterised by a fines-to-total aggregate ratio of 0.40 and a maximum aggregate size of 20 mm. Time-dependent behaviour was represented through a basic shrinkage strain of 0.000780 mm/mm, assuming moist curing conditions. Service-stage environmental conditions were defined by a relative humidity of 70%, an ambient temperature of 20°C, and an interior exposure class.

These assumptions are consistent with commonly reported values for precast prestressed elements and ensure realistic prediction of stress development and cracking behaviour.

3.3.3 Prestressing Tendon Properties

All prestressing tendons were modelled as high-strength steel strands with an ultimate tensile strength of 1790 MPa. Four tendon diameters—5 mm, 10 mm, 15 mm, and 20 mm—were considered in the parametric study.
For all slab configurations, the total prestressing steel area was kept constant. Consequently, variations in tendon diameter resulted only in changes in the number of tendons and their spatial distribution within the cross-section, without altering the total

prestressing force. This modelling strategy enables a direct and unbiased assessment of the influence of tendon diameter on cracking behaviour, flexural resistance, and compression-zone development.

3.4 Numerical Modelling in Concise Beam

Concise Beam was adopted as the primary numerical analysis tool due to its proven capability to simulate prestressed concrete members while accounting for sectional behaviour, material nonlinearity, and geometric effects. The hollow-core slabs were modelled with full geometric representation corresponding to slab depths of 200 mm, 320 mm, and 400 mm, including the actual void configuration and composite interaction with the cast-in-place topping.

Full composite action between the precast unit and the topping layer was assumed throughout the analysis. Concrete material nonlinearity was explicitly considered, including cracking initiation and post-cracking stiffness degradation. Prestressing tendons were modelled using the specified diameters and profiles, with prestress levels calibrated to ensure that the total prestressing steel area remained constant for all configurations.

All slabs were analysed under simply supported boundary conditions and subjected to a single concentrated load of 50 KN applied at mid-span, representing the critical flexural loading case. Incremental nonlinear analysis was performed up to failure, enabling the evaluation of cracking moment (M_{cr}), ultimate resistance moment (Mr), compression-zone depth (c), and curvature development along the span.

It should be noted that the cracking moment (M_{cr}) and resistance moment (M_r) presented in this study represent section capacity quantities, rather than internal bending moment demand. The distributions of $M_{cr}(x)$ and $M_r(x)$ correspond to the moment required to initiate first cracking and the ultimate flexural capacity of the section, respectively, evaluated at discrete locations along the slab length. Consequently, non-zero values at the slab ends (x = 0 and x = L) reflect the local flexural capacity of the prestressed section and do not imply the presence of bending moment demand at the supports.

3.5 Numerical Validation Using MATLAB

To verify the reliability of the Concise Beam simulations, independent numerical routines were developed in MATLAB based on classical sectional analysis. These routines incorporate nonlinear constitutive models for concrete and prestressing steel and were used to compute moment–curvature relationships, sectional stress and strain distributions, compression-zone depth evolution, and flexural capacity.

Identical geometric parameters, material properties, and prestressing steel areas were implemented in both Concise Beam and MATLAB to ensure consistency. The close agreement observed between the two sets of results provides confidence in the accuracy of the numerical model and confirms the suitability of Concise Beam for conducting the present parametric investigation.

3.6 Composite Slab Layout

All analysed slabs were modelled as fully composite members consisting of a precast hollow-core unit topped with a cast-in-place concrete layer. The composite section was defined by a clear span length of 12.0 m and a total width of 1220 mm. The precast unit thickness was taken as 70 mm, with the topping layer contributing to the overall flexural response.

Full composite action was assumed at the interface between the precast unit and the topping, with no relative slip permitted. The contribution of the topping layer was included in all sectional calculations, including the determination of cracking moment and ultimate flexural resistance.

4. RESULTS AND DISCUSSION

For clarity, the term 'moment distribution' used in the following sections refers to the spatial variation of flexural capacity along the slab, accounting for prestress level, eccentricity, and sectional properties. These distributions should not be interpreted as bending moment demand diagrams, which for a simply supported slab would be zero at the supports.

4.1 Behaviour under a Single Concentrated Load (50 KN at Mid-Span)

The following subsections present the cracking moments, flexural resistance, and compression depth results for the three slab thicknesses (200, 320, and 400 mm). For each case, the influence of tendon diameter is discussed while keeping the total tendon area constant.

Across all slab depths investigated (200, 320, and 400 mm), a consistent performance hierarchy was observed, with the 10 mm tendon configuration providing superior cracking resistance, flexural capacity, and compression-zone stability compared with larger tendon diameters. The following subsections therefore focus on how slab depth influences the magnitude of this response rather than repeating the same ranking.

4.1.1 Slab Thickness: 200 mm

Figure 1 shows the cracking moment distribution along the 200 mm slab subjected to a central concentrated load. Identical cracking moments of 38.95 KN.m are obtained at both slab ends (x = 0 and 12 m), consistent with the simply supported boundary conditions. Along the span, tendon diameter has a clear influence on cracking behaviour. The 10 mm tendons consistently provide the highest cracking moments, followed by the 15 mm configuration, while the 20 mm tendons exhibit the lowest values despite having the same total prestressing steel area. This reduced performance of larger tendons is attributed to the smaller number of strands, which leads to less uniform prestress distribution and localized stress concentrations. Overall, the results indicate that the 10 mm tendon configuration offers the most favourable cracking resistance for the 200 mm slab.

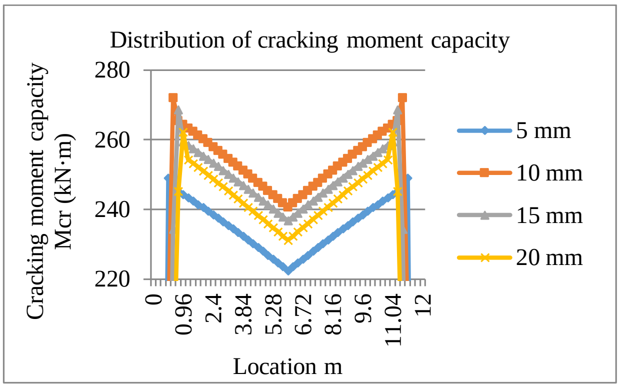

Figure 1. Cracking moment capacity (Mcr) distribution along the span for a 200 mm slab

Figure 2 illustrates the resistance moment distribution for the 200 mm slab subjected to a central concentrated load. All tendon configurations exhibit the characteristic flexural response of a simply supported member, with resistance increasing from the supports toward mid-span and decreasing symmetrically thereafter. The 10 mm tendons achieve the highest and most stable resistance over the central span region (approximately x = 3.36–8.64 m), while the 15 mm configuration shows slightly lower but comparable values. In contrast, the 5 mm tendons develop high resistance only over a limited span length, and the 20 mm tendons exhibit reduced resistance both near the supports and at mid-span. Overall, the results confirm that the 10 mm tendon configuration provides the most efficient and uniform flexural resistance profile for the 200 mm slab.

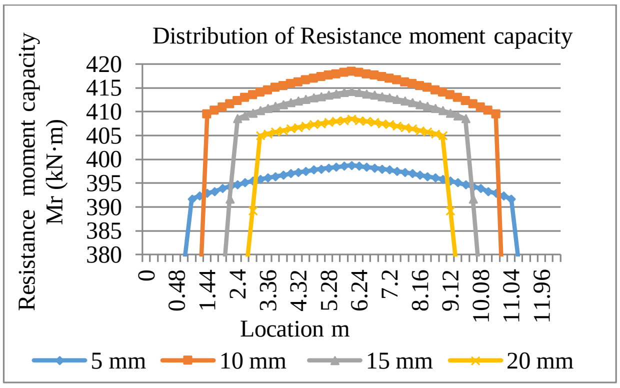

Figure 2. Resistance moment capacity (Mr) distribution along the span for a 200 mm slab

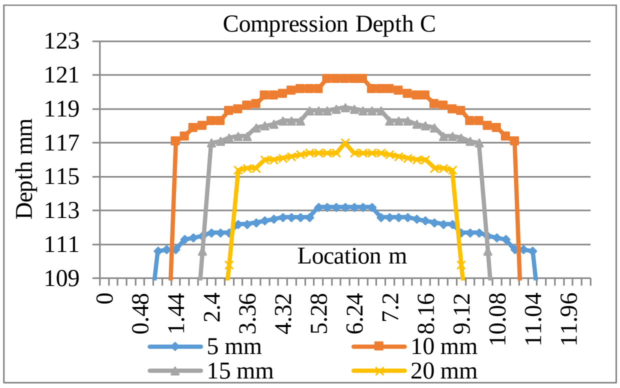

Figure 3. Compression-zone depth (c) distribution along the span for a 200 mm slab

Figure 3 presents the compression depth distribution for the 200 mm slab subjected to a central concentrated load. The observed trends are consistent with the flexural response discussed previously. The 10 mm tendon configuration develops the deepest and most uniform compression zone, reaching approximately 120 mm near mid-span, indicating an efficient internal force distribution. In contrast, the 5 mm tendons exhibit noticeable fluctuations in compression depth, reflecting greater sensitivity to curvature variations, while the 20 mm tendons produce the smallest and most localized compression zones, consistent with their lower cracking and resistance moments. Overall, the results confirm that the 10 mm tendons provide the most stable and favourable compression behaviour for the 200 mm slab.

4.1.2 Slab thickness: 320 mm

Figure 4 illustrates the cracking moment distribution for the 320 mm slab subjected to a central concentrated load. The same trend observed for the 200 mm slab is preserved. The 10 mm tendon configuration consistently provides the highest cracking moments along the entire span, while the 5 mm tendons result in the lowest values. The 15 mm and 20 mm tendons remain inferior to the 10 mm configuration at all locations. These results indicate that increasing slab depth does not change the fundamental influence of tendon diameter on cracking behavior, and that the 10 mm tendons continue to offer the most favorable cracking resistance.

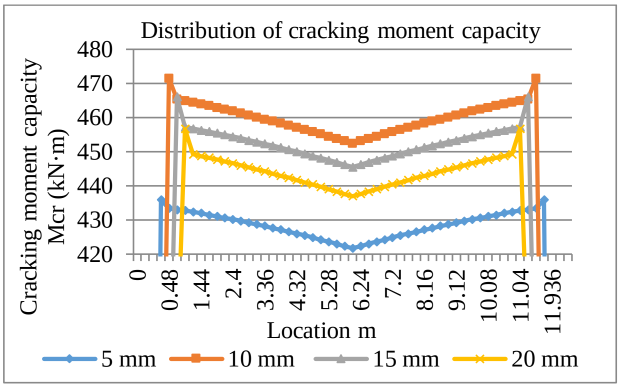

Figure 4. Cracking moment capacity (Mcr) distribution along the span for a 320 mm slab

Figures 5 and 6 present the resistance moment and compression-zone depth distributions for the 320 mm slab subjected to a central concentrated load. Consistent with the general response pattern identified across all slab depths, the flexural capacity and compression behaviour are strongly influenced by the manner in which the prestressing force is distributed along the section. Configurations characterised by a more uniform prestress distribution develop higher and more stable resistance levels over the central span region, accompanied by a deeper and more consistent compression zone. In contrast, configurations associated with a reduced number of larger tendons exhibit diminished flexural resistance and thinner compression zones, despite having the same total prestressing steel area. These observations indicate that prestress efficiency is governed primarily by the uniformity of force transfer rather than by tendon size alone, leading to improved flexural performance when prestressing is distributed over a greater number of tendons.

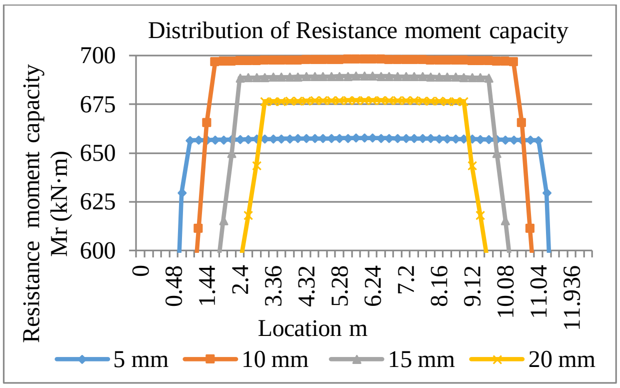

Figure 5. Resistance moment capacity (Mr) distribution along the span for a 320 mm slab

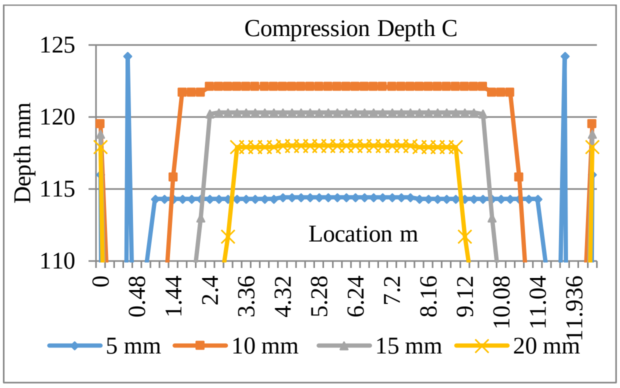

Figure 6. Compression depth (c) distribution along the span for a 320 mm slab

4.1.3 Slab thickness: 400 mm

Figure 7 illustrates the cracking moment distribution for the 400 mm slab subjected to a central concentrated load. Despite the increased slab depth, the same trend observed for the shallower slabs is maintained. The configuration with 10 mm tendons consistently provides the highest cracking moments along the span, whereas larger tendon diameters (15 mm and 20 mm) result in lower cracking resistance, even though the total prestressing steel area is unchanged. This behaviour confirms that increasing tendon diameter alone does not improve cracking performance when the prestressing steel area is kept constant.

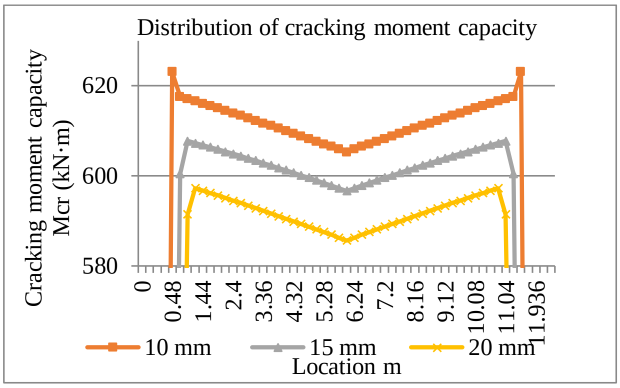

Figure 7. Cracking moment capacity (Mcr) distribution along the span for a 400 mm slab

Figure 8 presents the resistance moment distribution for the 400 mm slab subjected to a central concentrated load. The results clearly indicate a strong influence of tendon diameter on flexural capacity. The slab with 10 mm tendons achieves the highest mid-span resistance moment (approximately 639.6 kN·m), while the resistance decreases to about 547.4 kN·m and 450.3 kN·m for tendon diameters of 15 mm and 20 mm, respectively. In addition, the 10 mm tendon configuration maintains a wide region of high resistance across the central portion of the span (x ≈ 2.4–9.6 m), reflecting superior flexural efficiency and a more effective distribution of prestressing forces compared with larger-diameter tendons.

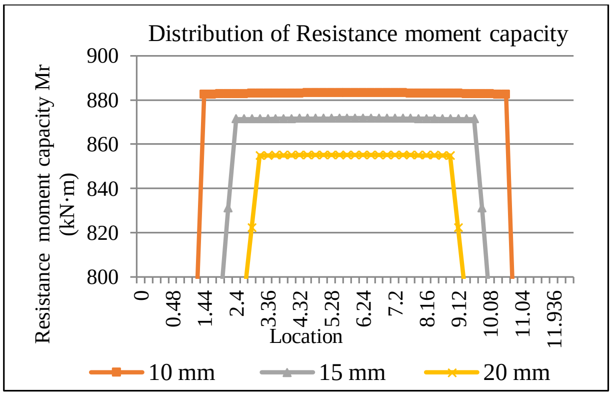

Figure 8. Resistance moment (Mr) distribution along the span for a 400 mm prestressed hollow-core slab

Figure 9 illustrates the compression depth distribution for the 400 mm slab subjected to a central concentrated load. Consistent with the behaviour observed for the 200 mm and 320 mm slabs, tendon diameter has a pronounced effect on compression-zone development.

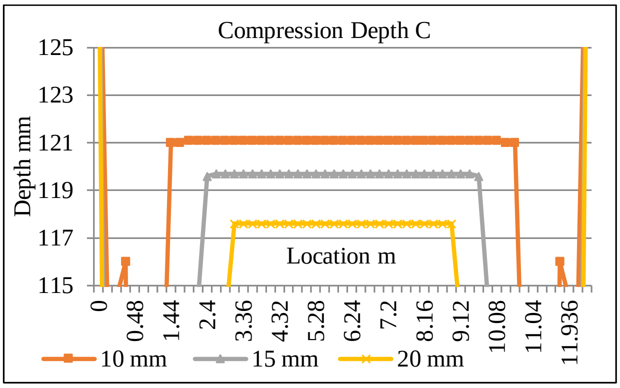

Figure 9. Compression-zone depth (c) distribution along the span for a 400 mm prestressed hollow-core slab

The 10 mm tendon configuration produces the largest and most stable compression depth along the span, varying approximately between 80 and 133 mm. In contrast, the compression zone becomes progressively thinner for larger tendon diameters, with minimum depths of about 58.6 mm for the 15 mm tendons and approximately 47.4 mm for the 20 mm tendons.

As shown in Figure 9, the reduction in compression depth for larger tendons corresponds directly with their lower cracking and resistance moments, confirming that distributing the prestressing force through a greater number of medium-diameter tendons leads to more effective utilisation of the concrete compression zone.

4.2 Validation using MATLAB

To confirm the accuracy of the Concise Beam simulations, independent MATLAB routines were developed using sectional analysis and nonlinear concrete constitutive models.

Table 4 presents a quantitative comparison between MATLAB and Concise Beam predictions of cracking moment at representative slab locations. The percentage differences are generally within 5% for all tendon diameters considered, with the maximum deviation occurring at mid-span where cracking capacity reaches its peak. Near the supports, the two approaches show nearly identical results. This level of agreement confirms the accuracy of the MATLAB sectional model and validates the use of Concise Beam for analysing the influence of tendon diameter on the flexural behaviour of prestressed hollow-core slabs.

Table 5 presents a quantitative comparison between MATLAB and Concise Beam predictions of the ultimate resistance moment at representative slab locations. The maximum differences occur near mid-span, where flexural resistance reaches its peak, and remain within approximately 5% for all tendon diameters considered. Near the supports, the two methods provide nearly identical values. This close agreement confirms the accuracy of the MATLAB sectional model and validates the reliability of Concise Beam in predicting flexural resistance for prestressed hollow-core slabs.

Table 3. Quantitative comparison of cracking moment (Mcr) obtained from Concise Beam and MATLAB at representative slab locations.

Position (m)	Tendon dia. (mm)	Concise Beam Mcr (kN·m)	MATLAB Mcr (kN·m)	Absolute diff. (kN·m)	Diff. (%)
0.0	10	38.95	38.95	0.00	0.0
6.0 (mid-span)	10	271.93	258.34	13.59	5.00
6.0 (mid-span)	15	226.12	214.81	11.31	5.00
6.0 (mid-span)	20	262.12	249.02	13.10	5.00
11.76	10	155.44	155.44	0.00	0.0

Table 4. Quantitative comparison of Resistance moment (Mr) obtained from Concise Beam and MATLAB at representative slab locations.

Position (m)	Tendon dia. (mm)	Concise Beam Mr (kN·m)	MATLAB Mr (kN·m)	Absolute diff. (kN·m)	Diff. (%)
0.0	10	0.39	0.39	0.00	0.0
6.0 (mid-span)	10	418.49	397.57	20.92	5.0
6.0 (mid-span)	15	353.16	335.01	18.15	5.1
6.0 (mid-span)	20	408.49	388.06	20.43	5.0
11.76	10	209.44	209.44	0.00	0.0

Figures 10–12 confirms a comparison between the results obtained from Concise Beam and the independent MATLAB calculations for cracking moment, resistance moment, and compression depth, respectively. For all tendon diameters and slab depths considered, the two sets of results show very close agreement in terms of overall trends, magnitude of response, and locations of peak values along the span. As illustrated in Figures 10–12, the MATLAB predictions consistently reproduce the Concise Beam results, confirming the robustness of the numerical implementation and the reliability of Concise Beam for assessing the influence of tendon diameter on the flexural behaviour of prestressed hollow-core slabs.

Figures 13–15 present the cracking moments, resistance moments, and compression-depth distributions obtained from the MATLAB analysis. The MATLAB results independently confirm that the 10 mm tendon configuration consistently achieves the highest cracking moments and flexural resistance, whereas the 15 mm and 20 mm tendon diameters lead to lower capacities. The compression-depth distributions shown in Figure 15 further support this observation, with the 10 mm tendons producing the deepest and most stable compression zone along the slab span.

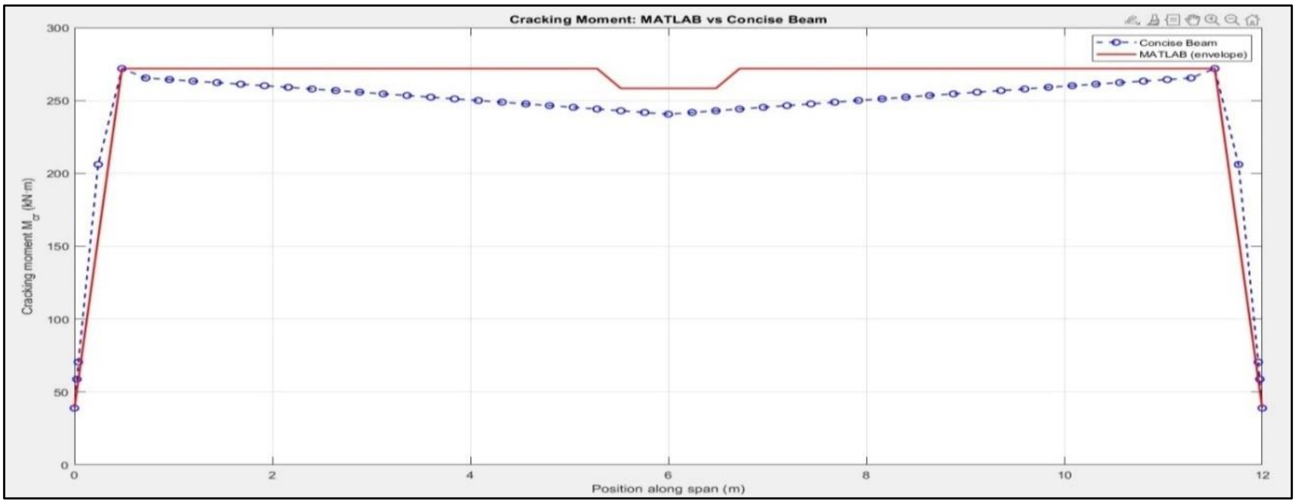

Figure 10. Cracking moments comparison MATLAB vs Concise beam

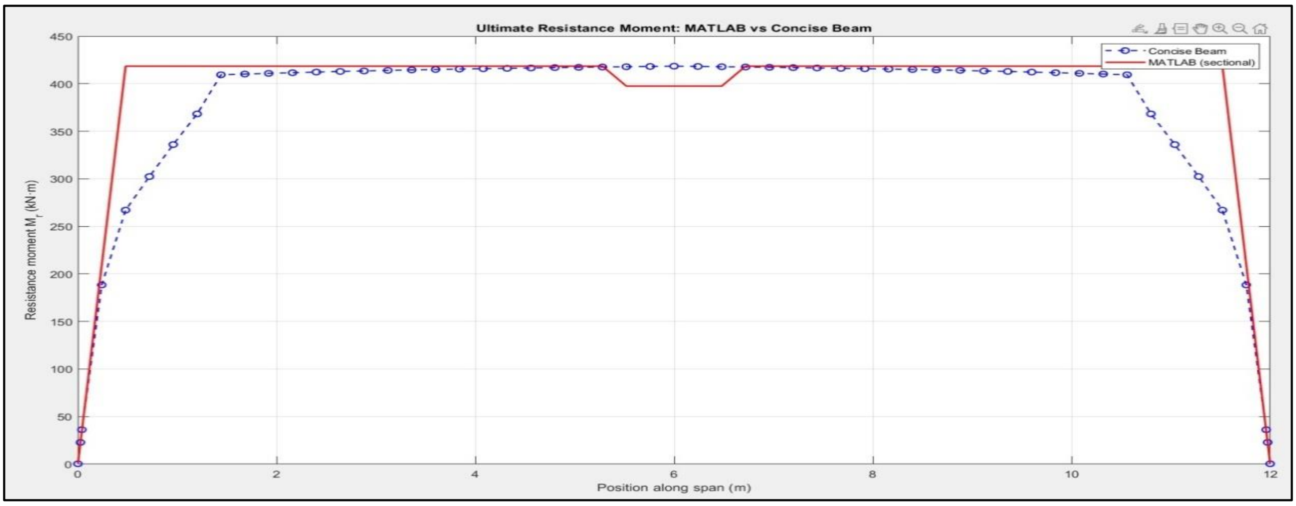

Figure 11. Resistance moments comparison MATLAB vs Concise beam

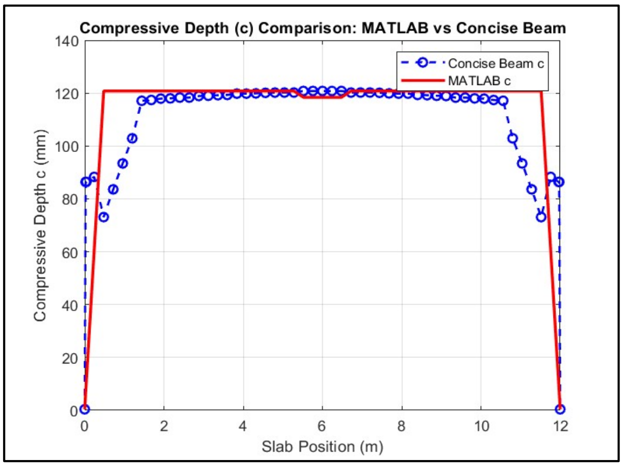

Figure 12. Compression depth comparison MATLAB vs Concise beam

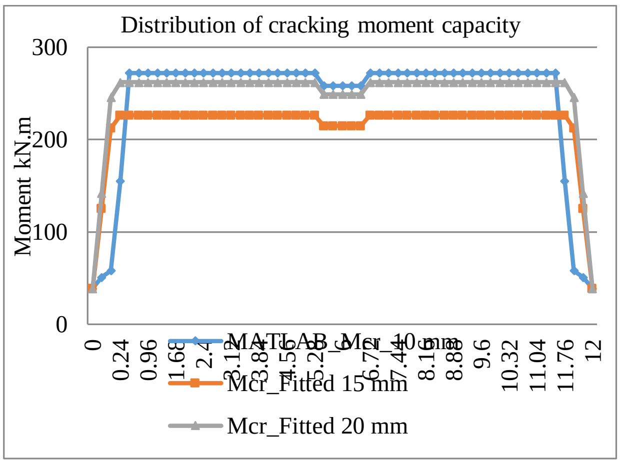

Figure 13. Cracking moments concluded from MATLAB

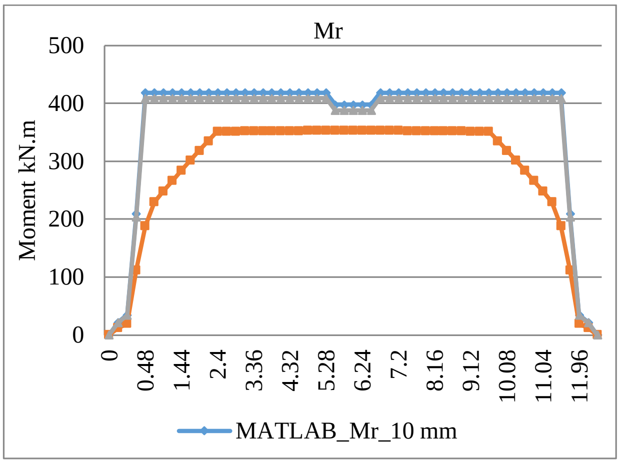

Figure 14. Resistance moments concluded from MATLAB

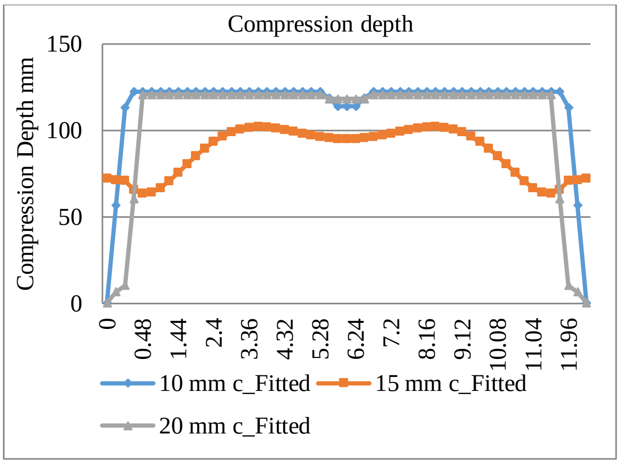

Figure 15. Compression depth concluded from MATLAB

The response trends predicted by MATLAB closely match those obtained from the Concise Beam simulations for all slab depths and tendon diameters considered. This strong consistency between the two independent numerical approaches validates the adopted modelling strategy and confirms that Concise Beam reliably captures the influence of tendon diameter on the flexural behaviour of prestressed hollow-core slabs.

5. CONCLUSION

This study investigated how tendon diameter influences the flexural behaviour of prestressed hollow-core slabs while keeping the total prestressing steel area constant. Numerical analyses were performed for slab depths of 200 mm, 320 mm, and 400 mm using Concise Beam, and key flexural response measures were independently checked through MATLAB-based sectional calculations (The MathWorks, Inc., 2023). The results confirm that tendon diameter remains an influential parameter even under a constant steel-area constraint, affecting the onset of cracking, stiffness evolution after cracking, and the development of the compression zone. These outcomes are consistent with the study focus and scope reported in recent work on varying tendon diameters and slab depths, and they reinforce the practical relevance of diameter selection during design and assessment (El Awady, 2025).

From a serviceability perspective, the analyses indicate that tendon arrangement through diameter selection can alter cracking resistance and the progression of flexural response, which aligns with the broader understanding that prestressing details significantly shape hollow-core slab behaviour (Al-Negheimish et al., 2018; McGinnis et al., 2024). Although the present work focused on flexure, the outcomes should be interpreted alongside prior findings that hollow-core performance is often governed by multiple interacting limit states, where shear behaviour and web-shear mechanisms may become decisive depending on geometry, detailing, and support conditions (Lee et al., 2020; Palmer & Schultz, 2010). In this sense, the trends observed here complement existing research by clarifying how tendon diameter can shift flexural response measures while the designer still needs to verify whether shear-related criteria control, as highlighted in recent evaluations of web-shear design procedures for hollow-core units (El-Sayed et al., 2022) and studies on factors affecting web-shear capacity (Asperheim & Dymond, 2021).

The findings also align with the wider direction of recent prestressed-slab research that combines numerical modelling with experimental evidence to understand bending, shear, and punching behaviour (McGinnis et al., 2024). The relevance of prestressing-related detailing choices in governing response is also consistent with recent work on post-tensioned hollow-core systems and the role of design assumptions in evaluating capacity and performance (Szydłowski et al., 2024; Elliott, 2021). At the practical level, this supports using tendon-diameter selection as part of serviceability-oriented decision making, while recognising that strengthening or intervention strategies are typically assessed with respect to cracking behaviour and the overall response of the unit (Abd Elhameed et al., 2024). More broadly, the emphasis on prestressing configuration and verification is consistent with parametric prestressing studies in other structural forms, which similarly show that tendon-related parameters can meaningfully alter global response and capacity predictions (Elbelbisi et al., 2022; Hasib et al., 2025).

Finally, while the present study provides a consistent numerical basis across multiple slab depths, it adopts modelling simplifications typical of parametric investigations, particularly regarding idealised composite action and tendon–concrete interaction, as well as simplified treatment of time-dependent effects. Given the documented sensitivity of prestressed systems to prestress losses and their influence on structural response, further work should incorporate more detailed loss modelling and validation against measured behaviour (He et al., 2024). Future research should also extend validation to conditions beyond ambient flexure, including elevated temperature scenarios where hollow-core slab performance can change substantially (Ellobody, 2014; Jeyashree et al., 2024). Overall, the study contributes a focused comparison of tendon-diameter effects under a controlled steel-area condition and provides a practical reference point for designers assessing prestressed hollow-core slabs alongside established flexural and shear considerations in the literature (Al-Negheimish et al., 2018; El-Sayed et al., 2022; Palmer & Schultz, 2010; Lee et al., 2020), with direct relevance to recent tendon-diameter-focused work (El Awady, 2025).

Acknowledgements: The authors acknowledge the use of Concise Beam software for the numerical analyses performed in this study. No external funding was received for this research.

Disclosure statement

This manuscript is an extended and substantially revised version of our earlier work that was made available as a preprint and presented at ICASGE’25 (2025) under the title “Load-bearing capacity: How varying tendon diameters influence the strength of prestressed concrete slabs of different depths.” The present submission expands the scope of the numerical study, adds additional outputs and discussion, and includes independent MATLAB-based calculations used to verify key flexural response measures. The earlier version is cited for transparency, and the current manuscript should be considered a significantly enhanced version rather than a duplicate publication.

References:

Abd Elhameed, A. E., Ali, E., Mahmoud, R., Eisa, A., El-Feky, M. H., Sabol, P., & Katunský, D. (2024). Strengthening of hollow core precast prestressed reinforced concrete slabs using different techniques. *Cogent Engineering, 11*(1). https://doi.org/10.1080/23311916.2024.2307170

Al-Negheimish, A. I., El-Sayed, A. K., Khanbari, M. O., & Alhozaimy, A. M. (2018). Structural behavior of prestressed SCC hollow core slabs. *Construction and Building Materials, 182*, 334–345. https://doi.org/10.1016/j.conbuildmat.2018.06.077

Asperheim, S. A., & Dymond, B. Z. (2021). Factors affecting web-shear capacity of hollow-core slabs with filled cores. *PCI Journal, 66*(4). https://doi.org/10.15554/pcij66.4-02

El Awady, M. A. A. E. M. (2025). *Load-bearing capacity: How varying tendon diameters influence the strength of prestressed concrete slabs of different depths* (Version 1). Research Square. https://doi.org/10.21203/rs.3.rs-6733926/v1

Elbelbisi, A. H., El-Sisi, A. A., Hassan, H. A., Salim, H. A., & Shabaan, H. F. (2022). Parametric study on steel–concrete composite beams strengthened with post-tensioned CFRP tendons. *Sustainability, 14*(23), 15792. https://doi.org/10.3390/su142315792

Elliott, K. S. (2021). Comparison of the design of prestressed concrete hollow-core floor units with eurocode 2 and ACI 318. *PCI Journal, 66*(2), 21–57. https://doi.org/10.15554/pcij66.2-01

Ellobody, E. (2014). Advanced analysis of prestressed hollow core concrete slabs exposed to different fires. *Advances in Structural Engineering, 17*(9). https://doi.org/10.1260/1369-4332.17.9.1281

El-Sayed, A. K., Al-Negheimish, A. I., Alhozaimy, A. M., & Al-Saawani, M. A. (2022). Evaluation of web shear design procedures for precast prestressed hollow core slabs. *Buildings, 13*(1), 23. https://doi.org/10.3390/buildings13010023

Hasib, S. I., Lateef, A. M., & Aziz, O. Q. (2025). Tendon profile layout impact on the shear capacity of unbonded post-tensioned prestressed concrete bridge I-girders. *Infrastructures, 10*(9), 222. https://doi.org/10.3390/infrastructures10090222

He, J., Wu, W., Tan, Z., Li, D., Cai, Y., & Guo, P. (2024). Analysis of the prestressing loss influence in prefabricated concrete bridges based on a drop weight impact method. *Buildings, 14*(12), 3961. https://doi.org/10.3390/buildings14123961

Jeyashree, T. M., Kannan, P. R., & Rajkumar. (2024). Investigation on performance of prestressed hollow core slabs exposed to elevated temperatures. *Journal of Structural Fire Engineering, 15*(3), 426–446. https://doi.org/10.1108/JSFE-09-2023-0037

Lee, Y.-J., Kim, H.-G., Kim, M.-J., Kim, D.-H., & Kim, K.-H. (2020). Shear performance for prestressed concrete hollow-core slabs. *Applied Sciences, 10*(5), 1636. https://doi.org/10.3390/app10051636

McGinnis, M. J., Gangone, M. V., Nogales, A., Gomez-Santana, L. M., Weldon, B., Reihl, A., Tošić, N., & Kurama, Y. (2024). Experimental and numerical investigation of the bending, shear, and punching shear behavior of recycled aggregate concrete precast/prestressed hollow core slabs. *Structural Concrete*. https://doi.org/10.1002/suco.202400008

Palmer, K. D., & Schultz, A. E. (2010). Factors affecting web-shear capacity of deep hollow-core units. *PCI Journal, 55*(2), 123–146. https://doi.org/10.15554/pcij.03012010.123.146

Szydłowski, R. S., Łabuzek, B., & Bednarski, Ł. (2024). Post-tensioned hollow-core concrete slabs with unbonded tendons for truck scale platforms: Design assumptions and tests. *Materials*, *17*(16), 4154. https://doi.org/10.3390/ma17164154

The MathWorks, Inc. (2023). *MATLAB* (Version R2023b) [Computer software]. Retrieved from https://www.mathworks.com/products/matlab.html

Mohamed A. El Awady
Faculty of Engineering, Heliopolis University, Cairo, Egypt
Dr.m_awady@yahoo.com
ORCID 0000-0003-2007-7075

Abdelrahman Elsaid
Faculty of Engineering, October 6 University, Giza, Egypt
Abdelrahman.Elsaid.Eng@o6u.edu.eg
ORCID 0009-0001-3134-168X

Mohamed Abdelhakim Basal
Faculty of Engineering, Civil Engineering Department, Menoufia University, Egypt
mohamedabdelhikeem@yahoo.com
ORCID 0000-0002-8842-8217